The Journal of Headache and Pain

RESEARCH

Open Access

Optogenetic inhibition of ventrolateral orbitofrontal cortex astrocytes facilitates ventrolateral periaqueductal gray glutamatergic activity to reduce hypersensitivity in infraorbital nerve injury rat model

Jaisan Islam[1†], Md Taufiqur Rahman[1†], Muhammad Ali[1], Hyong Kyu Kim[2], Elina KC[3] and Young Seok Park[1,4*]

Abstract

Background Trigeminal neuropathic pain (TNP) is a chronic condition characterized by heightened nociceptive responses and neuroinflammatory changes. While astrocytes are recognized as critical players in pain modulation, their specific role in influencing descending trigeminal pain pathways via ventrolateral orbitofrontal cortex (vlOFC) activity modulation remains underexplored. Therefore, we investigated the impact of optogenetic modulation of astrocytes in the vlOFC on pain hypersensitivity in a rat model of chronic constriction injury of the infraorbital nerve (CCI-ION).

Method Adult female Sprague Dawley rats underwent ION constriction to mimic TNP symptoms, with naive and sham animals serving as controls. AAV8-GFAP-hChR2-mCherry, AAV8-GFAP-eNpHR3.0-mCherry, or AAV8-GFAP-mCherry were delivered to the vlOFC for in vivo optogenetic manipulation. Pain behaviors were assessed using acetone, von Frey, and elevated plus maze tests, while electrophysiological recordings from the ventrolateral periaqueductal gray (vlPAG) and ventral posteromedial (VPM) thalamus were obtained.

Results Orofacial hyperalgesia, reduced vlPAG activity, and thalamic hyperexcitability were associated with vlOFC astrocytic hyperactivity in the TNP animals. In contrast, optogenetic inhibition of vlOFC astrocytes restored vlOFC glutamatergic signaling, increased vlPAG glutamatergic neuronal activity, and reduced hyperactivity in the VPM thalamus. Behavioral assessments also revealed alleviation of hyperalgesia, allodynia, and anxiety-like behaviors during the stimulation-ON phase, alongside reduced neuroinflammatory markers, including P2×3 and Iba-1.

[†]Jaisan Islam and Md Taufiqur Rahman contributed equally to this work.

*Correspondence:
Young Seok Park
youngseokparkmd@gmail.com

Full list of author information is available at the end of the article

However, astrocytic excitation and null virus controls did not alter TNP responses, underscoring the specificity of astrocytic inhibition.

Conclusion These findings suggest that the astrocytic subpopulation in the vlOFC and its robust influence on vlPAG glutamatergic neurons play a crucial role in restoring descending pain processing pathways, potentially contributing to the development of novel therapeutic approaches for TNP management.

Keywords Trigeminal neuropathic pain, Ventrolateral orbitofrontal cortex, Astrocytes, Ventrolateral periaqueductal gray, Optogenetics

Background

Trigeminal neuropathic pain (TNP) is a chronic and debilitating condition characterized by recurrent, severe pain in one or more branches of the trigeminal nerve, profoundly impairing patients' quality of life [21]. The pathophysiology of TNP involves a complex interplay between peripheral inputs originating from the trigeminal ganglion (TG) and central pain-processing regions, mediated by neurons, astrocytes, and microglia [9, 18, 25]. Among the central nervous system (CNS) regions implicated in pain modulation, recent evidence highlights the orbitofrontal cortex (OFC) as playing a significant role in processing the sensory and affective dimensions of pain, alongside its established functions in decision-making, emotion regulation, and reward processing. Notably, the ventrolateral OFC (vlOFC) has major glutamatergic projections to the ventrolateral periaqueductal gray (vlPAG), a key region in the descending pain processing pathway, suggesting its potential influence on pain modulation [17, 47].

Astrocytes, the most abundant glial cells in the CNS, are essential for maintaining homeostasis and supporting synaptic development [26]. They provide structural and metabolic support to neurons, influence neuronal networks through gliotransmitter release (e.g., ATP, glutamate), regulate extracellular ion concentrations, and modulate synaptic transmission, making them promising targets for restoring homeostasis in dysregulated neural networks [28, 37]. Emerging evidence indicates that astrocytes become hyperactive under chronic neuropathic pain (CNP) conditions, perpetuating pathological pain states [7, 10]. Although the role of astrocytes in TNP remains underexplored, our recent study demonstrated their critical involvement in sustaining TNP through activity in the trigeminal nucleus caudalis (TNC) [24]. However, their role in the descending pain processing pathway remains poorly understood. Therefore, investigating the functional role of astrocytes in the vlOFC may provide key insights for developing therapeutic strategies, particularly given the challenges posed by the TNC's deep brain location for direct neuromodulatory interventions in clinical applications.

The advent of optogenetic techniques has enabled precise in vivo manipulation of astrocyte activity using astrocyte-specific promoters and light-sensitive opsins. Recent studies demonstrated the feasibility of stimulating spinal astrocytes in live rats, highlighting the therapeutic potential of suppressing astrocyte hyperactivity for CNP management [2, 38]. Advances in non-invasive methods, such as transcranial light delivery and red-shifted ChrimsonR opsin, have further enhanced the feasibility of targeting cortical regions for clinical applications [4, 6, 30, 42, 45, 50, 54]. Therefore, investigating the functional role of astrocytes in the vlOFC, with its connections to the vlPAG, may provide critical insights into developing potential therapeutic strategies for TNP. This approach addresses the challenges of deep brain targeting and leverages astrocytic roles in neural regulation, positioning superficial brain regions as key targets for future interventions.

Here, we utilized an optogenetic approach to selectively modulate astrocytic activity in the vlOFC of a chronic constriction injury of the infraorbital nerve (CCI-ION) rat model. We demonstrated that inhibiting hyperactive astrocytes in the vlOFC alleviated TNP behaviors by modulating excitatory projections from the vlOFC to the vlPAG, thereby facilitating the descending pain processing network in TNP.

Methods

Animals

A total of 44 female Sprague Dawley rats, aged 8 weeks and weighing between 200 and 250 g, were obtained from Koatech Bio, South Korea. The rats were kept in ventilated cages with autoclaved wood chip bedding under controlled environmental conditions, including a temperature of 23 °C, a 12-hour light/dark cycle, and a humidity level of 30%. Standard rodent food and water were provided ad libitum, except during experimental sessions. All surgical procedures and behavioral assessments were conducted between 9:00 am and 6:00 pm. We exclusively used female animals, as trigeminal nerve injuries are known to occur more frequently in females compared to males [3].

CCI-ION surgery and stereotaxic injection of optogenetic virus

To establish the TNP model, 24 rats underwent CCI-ION surgery following baseline assessments, as previously described [21]. All the animals were randomly assigned into three groups: TNP ($n = 24$), sham ($n = 15$), and naïve-control ($n = 5$). For surgical procedures, general anesthesia was induced using intraperitoneal injections of 9 mg/kg xylazine (Rompun®, Bayer AG, Leverkusen, Germany) and 15 mg/kg Zoletil (Zoletil50®, Virbac Laboratories, Carros, France). A small incision was made along the curve of the frontal bone above the right eye to expose the ION. Using Dumont forceps, the ION was carefully separated from surrounding connective tissue and muscle by blunt dissection. After that, two ligatures, spaced 2–4 mm apart, were applied to the ION using 3 – 0 silk sutures. The incision was then closed with 3 – 0 silk sutures. The contralateral side was left unaltered in all rats. Sham-operated animals underwent the same surgical procedure without the placement of ligatures on the ION.

Following CCI-ION or sham surgery, the animals from both the TNP and sham groups were randomly divided into six subgroups: TNP-ChR2 ($n = 8$), TNP-NpHR ($n = 8$), TNP-Null ($n = 8$), Sham-ChR2 ($n = 5$), Sham-NpHR ($n = 5$), and Sham-Null ($n = 5$). Each animal was then placed on a stereotaxic platform (Model: 68025, RWD Life Science, Guangdong, China) for precise optogenetic viral injection. To specifically target astrocytes in the vlOFC, we utilized adeno-associated viruses (AAVs) containing a red fluorescent protein (mCherry) under the astrocyte-specific GFAP promoter. AAV8-GFAP-hChR2(H134R)-mCherry (8.14×10^13 GC/ml) and AAV8-GFAP-eNpHR3.0-mCherry (6.93×10^{13} GC/ml) optogenetic viruses were injected to express channelrhodopsin and halorhodopsin, respectively in the astrocytic populations, while AAV8-GFAP-mCherry (2.01×10^{14} GC/ml) served as the control or null virus. The viral vectors were provided by the KIST Viral Facility (Korea Institute of Science and Technology, Seoul, Republic of Korea). Under anesthesia, the body temperature of the animals was maintained at 36 °C using a heating pad throughout the procedure. Coordinates for the injection site were determined using the Paxinos rat brain atlas, with reference points defined as mediolateral (ML), anterior-posterior (AP) relative to the bregma, and dorsoventral (DV) from the pial surface. A small incision was made to expose the skull, and a 1 mm hole was drilled at the coordinates for vlOFC contralateral to the CCI-ION side (3.8 mm AP, -2 mm ML, -4.8 mm DV). Using a Hamilton syringe, the viral vectors were injected into the vlOFC at a rate of 0.2 µL/min using an automated microsyringe pump (KD Scientific Legato® 130 Syringe Pump, Harvard Apparatus, Holliston, MA, USA). Each animal received a 2 µL injection. To ensure proper viral diffusion and minimize leakage, the syringe was kept in place for five minutes after the injection. Once the needle was carefully withdrawn, the incision was sutured. All surgeries were conducted under aseptic conditions. After surgery, rats were housed individually in cages with sterile bedding to allow recovery and observed daily for the next five days. The experimental timeline and procedures are summarized in supplementary Fig. 1. Naïve-control animals did not undergo any surgical interventions.

Behavior tests

All behavioral assessments were conducted by a researcher blinded to the group assignments. Tests were performed one day before the CCI-ION surgery (baseline test) and subsequently every 7th day for three weeks post-surgery. Behavioral evaluations were completed over a two-day period each week. On the first day, the electronic von Frey (EVF) test was conducted first, followed by the cold hyperalgesia test. On the second day, the elevated plus maze test was performed. Each animal was given a two-hour rest period between tests, during which they were returned to their home cages.

Mechanical threshold test

Mechanical sensitivity of the ipsilateral orofacial region was assessed using an EVF machine (Electronic Von Frey, cat. no. 38450, including controller 38450-001 with software, and Von Frey Applicator 38450-004; Ugo Basile, China) [14, 51]. The EVF system is an improved alternative to traditional von Frey filaments, eliminating the need for multiple filaments and reducing experimenter bias by employing a hand-held force sensor with a rigid metal probe. This system enables a gradual and controlled application of force, with selectable ranges of 0–50 g, measured with 0.1 g sensitivity. The included software tools aid in applying force linearly using a rate-meter and slope adjustment, allowing precise detection of facial withdrawal thresholds. Following a 30-minute habituation period in a plexiglass cage, the EVF machine was brought near rats for adaptation. Rats were granted a short duration to investigate the filament before their removal. The stimuli were presented once the animals had acclimated to the filament's presence near the central area of the vibrissal pad within the ipsilateral ION area. The stimulation intensity was increased gradually. The minimum force (measured in grams) required to elicit pain-related or defensive behaviors, such as rapid withdrawal, escape attempts, biting, grabbing, or asymmetric facial stroking, was recorded [19]. Each test was repeated three times, and the mean threshold was calculated for analysis.

Cold Hyperalgesia Test

For the cold hyperalgesia assessment, the animals were placed in a plexiglass cage in a quiet environment for 30 min to allow habituation. A glass syringe was then used to apply a few drops of acetone to the ipsilateral vibrissal pad on the CCI-ION side of the face. Reflexive behaviors, such as rubbing or grooming of the ipsilateral facial region accompanied by vigorous head shaking, were observed and recorded for 2 min. Grooming or movements involving regions other than the orofacial area were excluded [19]. Each test was repeated three times with a five-minute interval, and the mean of the scores was calculated.

Elevated plus maze test

The elevated plus maze (EPM) test was conducted to evaluate anxiety-like behavior, following previously established protocols. The EPM consisted of two open arms (50 × 10 cm) and two closed arms (50 × 10 × 40 cm) extending from a central platform (10 × 10 cm), elevated 50 cm above the ground. After a 30-minute habituation period in a quiet environment, each rat was placed in the central platform of the maze, facing an open arm, and allowed to explore for 10 min. A video camera positioned overhead and Toxtrac software were used to track parameters such as the total distance traveled, the number of entries into open arms (OA) and closed arms (CA), and the time spent in each arm. An entry into an arm was defined as the animal crossing completely into the arm with all four paws. The percentage of time spent in the open arms (OA time%) and the percentage of open arm entries (OA entry%) were calculated as indicators of anxiety [19]. These were computed as follows:

$$\text{OA time}\% = (\text{OA time} / [\text{OA time} + \text{CA time}]) \times 100$$

$$\text{OA entry}\% = (\text{OA entries} / [\text{OA entries} + \text{CA entries}]) \times 100$$

These metrics provided a measure of the animal's aversion to open spaces, which reflects innate anxiety levels.

In vivo electrophysiology and optic fiber cannula implantation

To ensure optimal viral expression, in vivo recordings and fiber cannula implantation were conducted after three weeks of optogenetic virus injection. Extracellular recordings were performed on anesthetized rats (15 mg/kg Zoletil® and 9 mg/kg xylazine) inside a Faraday cage under quiet and low-light conditions. The animals were secured in a stereotaxic apparatus, and a craniotomy was performed above the vlPAG and VPM thalamic region at the coordinates: AP, -8 mm; ML, -0.6 mm; DV, -6.0 mm and AP, 3.5 mm; ML, 2.8 mm; DV, -6.0 mm, respectively. A fiber optic cannula (MFC_200/230–0.48_###_ZF2.5_A45, Doric Lenses, Quebec City, Quebec, Canada) was placed stereotaxically, positioned 0.2 mm dorsal to the viral injection site in the vlOFC. For extracellular recordings, a quartz-insulated carbon microelectrode (E1011-20, Carbostar-1, Kation Scientific, Minneapolis, MN, USA) was first stereotaxically placed in the vlPAG ipsilateral to the optic fiber and subsequently in the VPM thalamus contralateral to the optic fiber. Ground and reference wires were anchored to the skull screws, connecting the electrode to an electronic interface board (EIB-36, Neuralynx, USA).

Neuronal signals from the vlPAG and VPM were acquired using the Cheetah Acquisition System (Neuralynx, USA) connected to the EIB-36 headstage and preamplifiers. Data were processed with a Digital Lynx SX data acquisition system (Neuralynx, Bozeman, USA), with signals filtered between 0.9 and 5 kHz and a sampling rate of 32 kHz [24]. Acute evoked recordings, were performed during alternating light-off and light-on conditions in the vlOFC. Evoked responses were triggered by applying a 10 g von Frey filament to the ipsilateral whisker pad. Each recording session lasted approximately two hours without the need for additional anesthesia. Once the recording from both vlPAG and VPM were performed, the cannula was affixed to the skull using dental cement and Superbond (Ortho-jet Pound Package, Lang Dental, Wheeling, IL, USA). Following the recordings, animals were allowed a seven-day recovery period in their home cages before subsequent experiments.

The recorded data were analyzed using Spikesort 3D software to isolate and identify distinct waveform clusters. Single units were defined as distinct extracellularly recorded neuronal spikes that exhibited a consistent waveform shape, peak-to-peak amplitude, and clear refractory periods, ensuring they originated from individual neurons rather than multi-unit activity. Only well-isolated clusters with stable firing properties were considered for further analysis. These single-unit activities were exported to NeuroExplorer (version 5, Nex Technologies, Colorado Springs, USA). This software enabled comprehensive spike train analysis, including rate histograms, raster plots, and burst analyses. Burst firing was defined as a group of at least three spikes with a maximum interval of 4 ms between spikes, with an interval of 100 ms between bursts. Inter-spike interval histograms were used to ensure consistency in burst pattern comparisons among groups.

Optogenetic modulation parameters

For the NpHR groups, we used a diode-pumped solid-state (DPSS) laser emitting yellow light at a 593 nm wavelength (Model: YL589T3-010FC, Shanghai Laser & Optics Century Co. Ltd., Shanghai, China), connected to

a monofiber optic patch cord. Yellow light with an output power of 10 mW was supplied for 5 min using a power supply (ADR-700D; ADR, Shanghai, China). The laser's power and waveform were controlled using a waveform generator (Keysight 33511B-CFG001; Keysight, Santa Rosa, CA, USA). For optical stimulation, we employed a 20 Hz frequency, and 4 ms pulse width. Animals were subjected to continuous 593 nm illumination at a minimum irradiance of 0.4 mW/mm^2 to ensure complete spiking inhibition (Bansal et al., 2020).

For the ChR2 groups, a laser power supply emitting blue light at a 473 nm wavelength (BL473T3-100, ADR-700D, Shanghai, China) was used in conjunction with the waveform generator to regulate the waveform and pulse width of the laser. The laser was set to an intensity of 10 mW, a pulse width of 4 ms, and a pulse frequency of 20 Hz [2,14,69]. Intermittent blue light was delivered via the cannula optic fiber equipped with a rotary joint patch cable.

Behavior tests with optic stimulation

One week after completing the electrophysiological experiments, the animals were taken to the behavioral assessment area again and allowed to habituate for 30 min before the testing session began. Behavioral tests were conducted during both laser stimulation (on) and non-stimulation (off) conditions. For five minutes, vlOFC astrocytes were either inhibited with yellow laser light or stimulated with blue laser light, after which the behavioral tests were conducted under the same conditions. In both stimulation-off and on instances, the tethered fiber system and associated equipment were connected during the procedure.

Immunostaining and histological examination

All the animals were exposed to optogenetic stimulation for 10 min before being deeply anesthetized using a Zoletil/xylazine mixture. Transcardial perfusion was performed using PBS followed by 4% paraformaldehyde (PFA). The brain and trigeminal ganglia (TG) were extracted, fixed in 4% PFA overnight, and subsequently immersed in a 30% sucrose solution. The tissues were cryopreserved and embedded in an optimal cutting temperature (OCT) compound (Tissue Tek®, Sakura, USA). Cryostat Sect. (20 μm thick) were prepared for immunostaining. The sections were fixed in acetone for 10 min, blocked with 10% normal goat serum at room temperature for 1 h, and incubated overnight at 4 °C with primary antibodies: mouse anti-GFAP (1:250, ab68428, Abcam), mouse anti-c-fos (1:1000, ab208942, Abcam), mouse anti-Iba1 (1:100, ab283319, Abcam), and mouse anti-CGRP (1:50, ab81887, Abcam), rabbit anti-VGLUT2(1:250, ab216463, Abcam). Following washes, the sections were incubated at room temperature for 2 h with secondary antibodies conjugated to Alexa Fluor 488 (ab150077, ab150113, Abcam, ab 150080). DAPI-containing mounting medium (H-2000, Vectashield®, Vector Laboratories Inc., Burlingame, CA) was used to mount the sections with coverslips. Imaging was performed using a fluorescence microscope equipped with cellSens Standard or OlyVia 2.4 software (Olympus Corp., Tokyo, Japan).

For quantitative analysis, three coronal sections from each targeted region were selected for each immunohistochemical marker. mCherry fluorescence intensity was quantified by measuring the red channel signal. A reference region near the injection site was used to establish background fluorescence, which was subtracted from the integrated density to calculate the corrected total cell fluorescence (CTCF). ImageJ software (National Institutes of Health, MD, USA) was employed to measure and compare the mean fluorescence intensity across groups.

To evaluate P2 × 3 expression in the TNC, chromogenic immunohistochemistry was performed. Frozen sections fixed in acetone were pre-incubated for one hour in 2.5% normal horse serum before incubation with a recombinant anti-P2 × 3 antibody (1:50, ab300493, Abcam) overnight at 4 °C. After washing, the sections were treated with biotinylated anti-mouse/rabbit IgG and processed using an avidin-biotin HRP detection system with an ABC kit (PK-7200, Vector Laboratories, Burlingame, CA) and DAB substrate kit (SK-4100, Vector Laboratories, Burlingame, CA). P2 × 3 expression was quantified using the color detection feature in the immunohistochemical image analysis toolbox of ImageJ software.

Statistical analysis

The data are expressed as mean ± standard deviation (SD). Sample sizes were determined using G*Power software (version 3.1.9.4, Germany) and prior experimental considerations. Rats with inadequate viral expression were excluded from the study. Statistical analyses were performed using ordinary one-way ANOVA (for equal group size), non-parametric repeated measures Friedman test, or non-parametric Kruskal-Wallis test (for unequal group size) to compare three or more different groups. For comparisons between two groups, either a paired *t*-test or an unpaired *t*-test was used, depending on the experimental condition. Statistical significance was indicated as follows: $^{*}P < 0.05$, $^{**}P < 0.01$, $^{***}P < 0.001$, and $^{****}P < 0.0001$. All statistical evaluations were carried out using GraphPad Prism software (version 9.1.0, Inc., San Diego, CA, USA).

Results

Behavioral hypersensitivity and upregulation of vlOFC astrocytes post-CCI-ION surgery

Following the CCI-ION surgery, animals in the TNP group exhibited persistent mechanical hypersensitivity,

heightened nocifensive behavior, and anxiety-like symptoms across all behavioral response analyses, while animals in the sham and naïve-control groups displayed negligible alterations, indicating a successful establishment of the TNP model (Fig. 1, Supplementary Table 1). The experimental timeline for behavioral testing and the surgical procedure for CCI-ION are illustrated in Fig. 1A and B, respectively.

The mechanical threshold measured by the EVF revealed a progressive decrease in the mechanical threshold in TNP animals over three weeks post-surgery, from 13.22 ± 1.19 gm to 8.23 ± 1.60 gm (non-parametric repeated measures Friedman test, Friedman

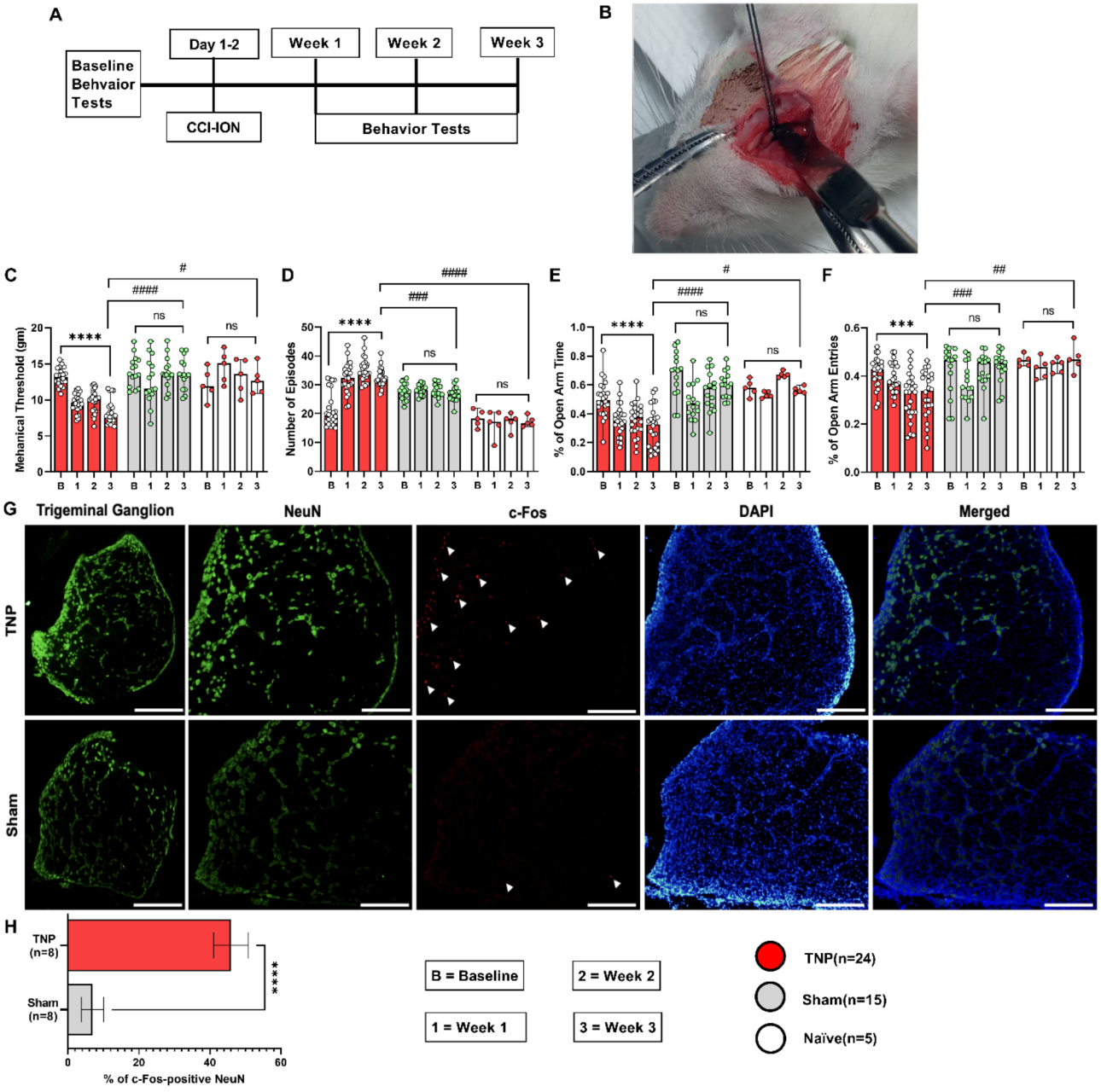

Fig. 1 Behavioral hypersensitivity after CCI-ION surgery. (**A**) Behavior tests conducting timeline. (**B**) CCI-ION model making procedure. (**C**) Ipsilateral orofacial mechanical withdrawal threshold measured by EVF machine. **(D)** Ipsilateral orofacial cold hyperalgesia score with cold acetone drops. **(E-F)**. Results of the elevated plus maze test; Time spent in open arm in % (**E**); Total entries in the open arm in % (**F**). *** $p < 0.001$, **** $p < 0.0001$; non-parametric repeated measures Friedman test analysis within the same group. # $p < 0.05$, ## $p < 0.01$, ### $p < 0.001$, #### $p < 0.0001$; non-parametric Kruskal-Wallis analysis among different groups. Data are presented as the mean ± SD. (**G**) c-Fos and NeuN positive immunostaining and their colocalization from the trigeminal ganglion of the TNP and sham groups. Scale bar = 200 µm (whole section); 100 µm (magnified section). **(H)** Quantification of c-Fos-positive NeuN in the trigeminal ganglion of the TNP ($n = 8$) and sham ($n = 8$) groups. Data are presented as the mean ± SD; unpaired *t*-test, **** $P < 0.0001$

statistic = 52.05, $p < 0.0001$; Fig. 1C). In comparison, the mechanical thresholds of the sham (13.60 ± 2.10 g) and naïve-control groups (12.75 ± 1.76 g) remained relatively unchanged, indicating that CCI-ION specifically induced mechanical hypersensitivity.

The CH score increased substantially in TNP animals, rising from 21.57 ± 5.96 to 32.58 ± 3.02 (non-parametric repeated measures Friedman test, Friedman statistic = 48.15, $p < 0.0001$; Fig. 1D) during the three-week observation period. This score was significantly higher in TNP animals compared to sham (26.74 ± 2.60) and naïve-control groups (17.24 ± 1.59), highlighting enhanced nocifensive behavior due to CCI-ION.

In the EPM test, TNP animals showed a marked reduction in both OAT and OAE scores, measures of anxiety-like behavior. The OAT decreased from 0.50 ± 0.12 s to 0.31 ± 0.14 s (non-parametric repeated measures Friedman test, Friedman statistic = 34.36, $p < 0.0001$; Fig. 1E), and the OAE declined from 0.42 ± 0.06 to 0.32 ± 0.09 (non-parametric repeated measures Friedman test, Friedman statistic = 26.07, $p < 0.001$; Fig. 1F) by the third week. Sham and naïve-control groups exhibited significantly higher OAT (0.60 ± 0.08 s, 0.56 ± 0.02 s) and OAE (0.44 ± 0.06, 0.47 ± 0.05) scores, suggesting that the CCI-ION induces anxiety-like behavior commonly associated with TNP.

IFC analysis revealed heightened expression of c-Fos, a marker of neuronal activation, co-localized with NeuN in the TG of TNP animals. This finding indicates elevated TG activity, likely contributing to the modulation of the TNP sensory pathway. In contrast, the sham group showed minimal or insignificant c-Fos-positive NeuN expression in the TG (Fig. 1G and H). In addition, we observed a marked increase in active CGRP expression in the TG of TNP animals (Supplementary Fig. 2). CGRP, a neuropeptide implicated in nociceptive signaling and neurogenic inflammation, is known to play a crucial role in the sensitization and transmission of pain signals within the trigeminal system. This elevated CGRP expression was not observed in sham-operated animals, highlighting its specific association with the TNP condition induced by CCI-ION.

IFC analysis also revealed a significant upregulation of GFAP expression in the vlOFC of TNP animals, indicating enhanced astrocytic activation (Fig. 2A-D). This upregulation was notably absent or minimal in the vlOFC of sham-operated (Fig. 2E-H) and naïve-control (Fig. 2I-L) animals, underscoring the specificity of astrocytic responses to the CCI-ION surgery. Quantitative analysis demonstrated a significantly marked increase in the number of GFAP-labeled astrocytes in the vlOFC of TNP animals three weeks post-CCI-ION compared to sham and naïve groups (Fig. 2M). These findings align with previous studies suggesting that astrocytic activation is a hallmark of trigeminal nerve injury, commonly associated with behavioral hyperalgesia [24, 41].

Inhibition of vlOFC astrocytic activity alleviates TNP behavioral responses

To investigate the role of astrocytic activity in the vlOFC in modulating TNP, we employed astrocyte-specific viral constructs using AAV8 engineered with a GFAP promoter. These constructs drove the expression of either the inhibitory opsin eNpHR3.0-mCherry, the excitatory opsin hChR2(H134R)-mCherry, or a control vector mCherry (Fig. 3A). Unilateral viral injections were performed in the vlOFC, and transduction efficiency was assessed seven weeks post-injection. mCherry fluorescence intensity analysis showed no significant differences among groups, confirming comparable viral expression (Supplementary Fig. 3).

The astrocyte specificity of the viral constructs was validated by the co-localization of mCherry with GFAP. Analysis revealed active GFAP expression in the vlOFC areas transduced with ChR2 and Null viruses, while significantly lower GFAP expression was observed in regions transduced with the NpHR virus (Fig. 3B and C). These findings indicate that NpHR-mediated optogenetic stimulation effectively suppressed astrocytic activity in the vlOFC.

To evaluate the impact of astrocytic modulation on TNP-related behaviors, animals underwent behavioral tests under both optic stimulation-off and stimulation-on conditions. Optic stimulation was initiated three minutes before and continued throughout the duration of the behavior tests during the stimulation-on condition. The TNP-NpHR group exhibited significant improvements in all behavioral parameters during the stimulation-on condition compared to stimulation-off. In the EVF test, the mechanical threshold increased from 9.68 ± 0.89 g (stimulation-off) to 11.20 ± 0.81 g (stimulation-on; paired *t*-test, (t, df) = (5.342, 7), $p < 0.01$; Fig. 3D). Similarly, the CHT score decreased from 38.92 ± 3.61 to 32.13 ± 2.28 (paired *t*-test, (t, df) = (3.685, 7), $p < 0.01$; Fig. 3E). In the EPM test, the open arm time (OAT) increased from 0.36 ± 0.1 to 0.44 ± 0.05 (paired *t*-test, (t, df) = (2.831, 7), $p < 0.05$; Fig. 3F), while open arm entries (OAE) increased from 0.38 ± 0.07 to 0.49 ± 0.04 (paired *t*-test, (t, df) = (4.701, 7), $p < 0.0$; Fig. 3G). The representative trajectory of TNP-ChR2, TNP-NpHR, and TNP-Null groups in the EPM test are shown in Fig. 3H-J, respectively.

In contrast, no significant alterations were observed in behavioral scores of the TNP-ChR2, TNP-Null, Sham-ChR2, Sham-NpHR, and Sham-Null groups under optic stimulation (Fig. 3D-G; Supplementary Table 2). This suggests that inhibition of astrocytic activity in the vlOFC via NpHR has a significant antinociceptive effect in TNP conditions. The absence of behavioral changes in the

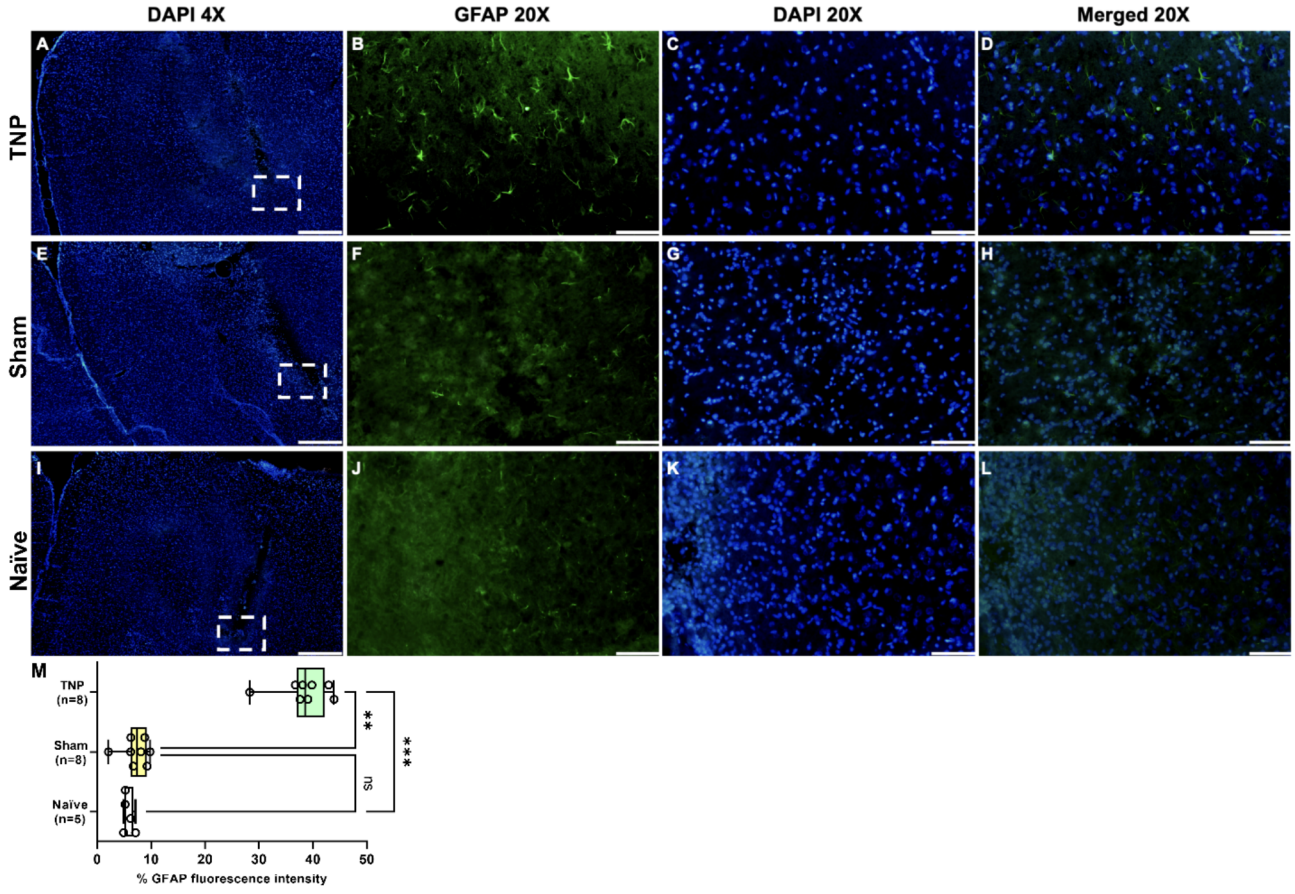

Fig. 2 CCI-ION surgery-induced astrocytic hyperactivation in the vlOFC. **(A-D)** Representative immunofluorescence image of GFAP-positive expression in the vlOFC of the TNP group. **(E-H)** Representative immunofluorescence image of GFAP-positive expression in the vlOFC of the sham group. **(I-L)** Representative immunofluorescence image of GFAP-positive expression in the vlOFC of the naïve-control group. Scale bar = 200 µm (**A, E, I**); 50 µm (**B-D, F-H, J-L**). **(M)** Quantification of GFAP expression in the vlOFC from TNP ($n = 8$), sham ($n = 8$), and naïve-control ($n = 5$) groups; non-parametric Kruskal-Wallis test analysis, Kruskal-Wallis statistic = 15.20, ** $p < 0.01$, *** $p < 0.001$. Data are presented as the mean ± SD

ChR2 group likely reflects a ceiling effect, as astrocytes in the TNP condition are already in a hyperactive state, and further activation did not enhance sensitivity. Similarly, the null virus group, which lacks the functional modification of astrocytes, served as a control and did not induce any behavioral changes.

Inhibition of vlOFC astrocytic activity enhances vlOFC-vlPAG glutamatergic projections and facilitates vlPAG activity

To explore the role of vlOFC astrocytes in modulating descending pain pathways, we investigated how astrocytic inhibition affects neural activity in the vlPAG. Using in vivo single-unit extracellular recordings, we assessed vlPAG firing rates and burst activity in both sham and TNP animals (Fig. 4A and B). Following CCI-ION surgery, TNP animals exhibited a significant reduction in both the mean firing rate and burst firing activity of vlPAG neurons compared to sham animals (Fig. 4C and D). This diminished vlPAG activity aligns with the impaired descending pain modulation observed in neuropathic pain states.

Optogenetic inhibition of astrocytic activity in the vlOFC, achieved via GFAP-NpHR-mediated stimulation, significantly restored vlPAG neuronal activity in TNP-NpHR animals. During optic stimulation-on conditions, the mean firing rate of vlPAG neurons increased from 9.77 ± 2.40 Hz to 12.78 ± 2.43 Hz (paired *t*-test, (t, df) = (3.645, 7), $p < 0.01$; Fig. 4E), and burst firing activity rose from 0.06 ± 0.03 bursts/s to 0.11 ± 0.02 bursts/s (paired *t*-test, (t, df) = (4.592, 7), $p < 0.01$; Fig. 4F). Furthermore, vlOFC astrocytic inhibition enhanced firing frequency (impulses per second) and increased burst traces in the vlPAG of TNP-NpHR animals, as shown in Fig. 4G and H. In contrast, optogenetic stimulation of vlOFC astrocytes in TNP-ChR2 and TNP-Null groups did not alter vlPAG neuronal activity, suggesting that suppression of astrocytic activity, rather than its activation, is key to restoring descending pain modulation in TNP conditions (Supplementary Table 3).

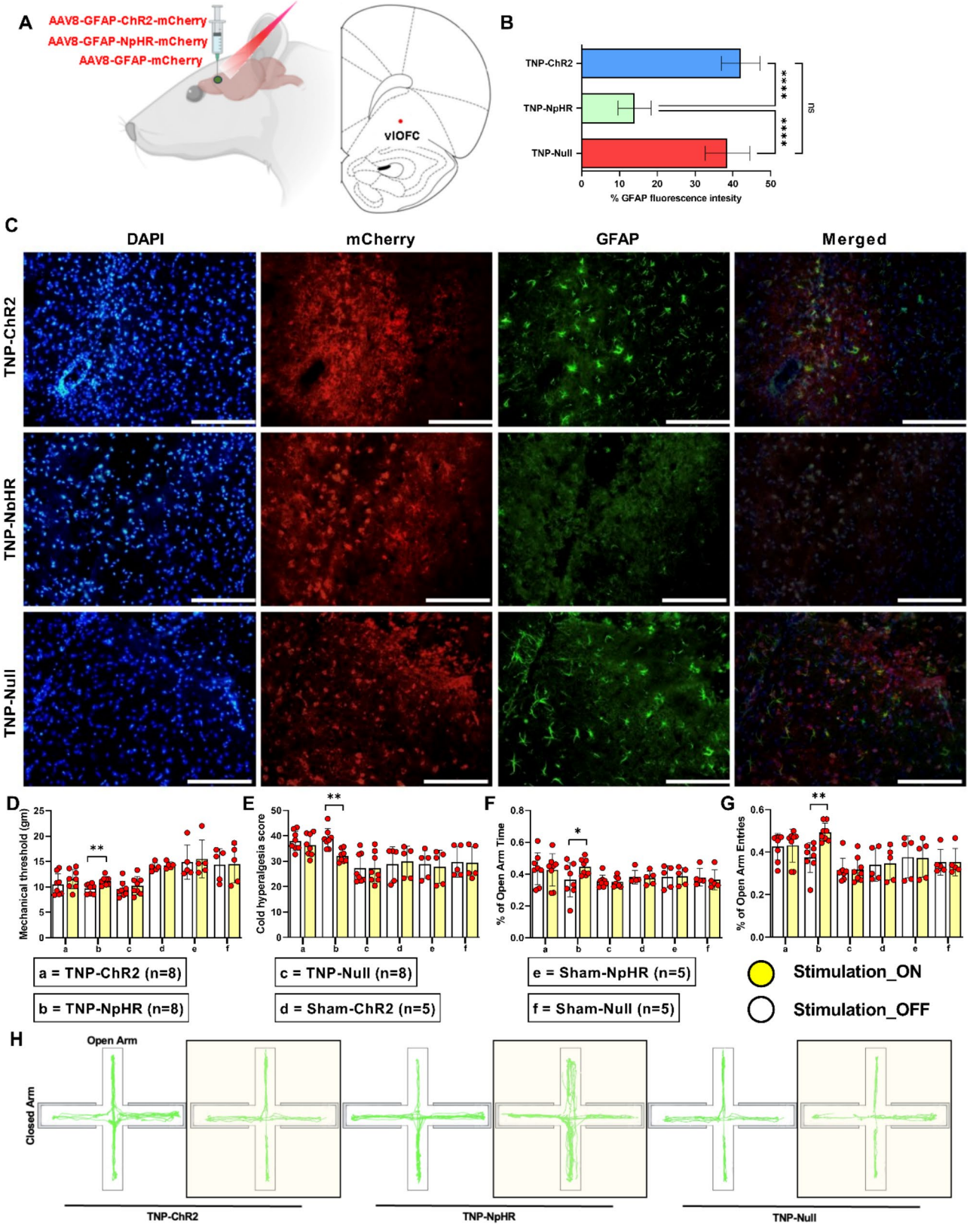

Fig. 3 (See legend on next page.)

(See figure on previous page.)

Fig. 3 Optogenetic inhibition of the vlOFC astrocytes attenuates pain hypersensitivity and associated anxiety behaviors. **(A)** Schematic representation of viral vector injections and optic stimulation in the vlOFC. **(B)** Quantification of GFAP fluorescence intensity (%) in TNP-ChR2 ($n = 8$), TNP-NpHR ($n = 8$), and TNP-Null ($n = 8$) group in response to optic stimulation; ordinary one-way ANOVA analysis, F (2, 21) = 69.91, **** $p < 0.0001$. Data are presented as the mean ± SD. **(C)** Representative immunofluorescence image of colocalized GFAP expression and mCherry expression in TNP-ChR2, TNP-NpHR, and TNP-Null group; scale bar = 50 µm. **(D)** Ipsilateral orofacial mechanical withdrawal threshold with optic stimulation off and on condition from different groups (paired *t*-test). **(E)** Ipsilateral orofacial cold hyperalgesia score with optic stimulation off and on condition from different groups (paired *t*-test). **(F)** Time spent in open arms of the EPM with optic stimulation off and on condition from different groups (paired *t*-test). **(G)** Number of entries in the open arms of the EPM with optic stimulation off and on condition from different groups (paired *t*-test). **(H)** Representative trajectory images of TNP groups in the EPM with optic stimulation off and on condition

To validate these findings, we performed IFC analysis of glutamatergic neurons in both the vlOFC and vlPAG. Optogenetic inhibition of astrocytic activity in the vlOFC significantly increased the expression of glutamatergic neurons in the vlOFC of TNP-NpHR animals compared to TNP-ChR2 and TNP-Null groups (Supplementary Fig. 4). This heightened glutamatergic activity in the vlOFC subsequently influenced glutamatergic projections to the vlPAG, as reflected by increased glutamatergic activity in the vlPAG of TNP-NpHR animals (Fig. 4I-K).

These results provide robust evidence that astrocytic inhibition in the vlOFC facilitates descending pain modulation through enhanced vlOFC-vlPAG glutamatergic signaling. Increased glutamatergic activity in the vlOFC stimulates vlPAG neurons, thereby improving descending pain processing and alleviating nociceptive hypersensitivity in TNP animals.

Inhibition of vlOFC astrocytic activity reduces VPM neural discharge

To investigate the influence of vlOFC astrocytic activity on spinothalamic nociceptive processing, we recorded neural activity from the VPM thalamus, a critical relay in pain signaling pathways (Fig. 5A and B). TNP animals exhibited significantly heightened tonic firing and burst firing rates in the VPM compared to sham animals, indicative of enhanced nociceptive transmission (Fig. 5C and D, respectively). This increased neuronal activity reflects the hyperexcitable state of the VPM thalamus in TNP conditions, consistent with its role in amplifying pain perception.

Then we performed VPM thalamic recording with optic stimulation off and on conditions. Optogenetic inhibition of astrocytic activity in the vlOFC, mediated by GFAP-NpHR, significantly reduced VPM neural activity in TNP-NpHR animals. During optic stimulation-on conditions, the mean firing rate of VPM neurons decreased compared to the stimulation-off condition (from 27.37 ± 3.76 Hz to 14.72 ± 2.68 Hz (paired *t*-test, (t, df) = (6.864, 7), $p < 0.001$; Fig. 5E), demonstrating a clear suppression of hyperactive thalamic output. Similarly, burst firing rates in the VPM were significantly attenuated following inhibition of vlOFC astrocytes (from 0.17 ± 0.03 to 0.08 ± 0.03 bursts/s (paired *t*-test, (t, df) = (4.646, 7), $p < 0.01$; Fig. 5F), further supporting the modulatory influence of vlOFC astrocytic inhibition on thalamic activity. Additionally, vlOFC astrocytic activity inhibition decreased firing frequency (impulses per second) and reduced burst traces in the VPM thalamus of TNP-NpHR animals, as illustrated in Fig. 5G and H, respectively. In contrast, optogenetic stimulation of vlOFC astrocytes in TNP-ChR2 and TNP-Null groups did not alter VPM thalamic activity, suggesting that suppression of vlOFC astrocytic activity, rather than its activation, is a potential approach to modulating spinothalamic projections and reducing nociceptive VPM thalamic hyperactivity in TNP conditions (Supplementary Table 4).

To validate the electrophysiological findings, we analyzed c-Fos expression, a marker of neuronal activation, in the VPM thalamus. Optogenetic inhibition of vlOFC astrocytes in the TNP-NpHR group significantly reduced c-Fos expression compared to the TNP-ChR2 and TNP-Null groups (Fig. 5I-K), confirming the suppression of VPM thalamic hyperactivity.

These results indicate that vlOFC astrocytic inhibition mitigates VPM thalamic hyperactivity, as evidenced by decreased firing rates and neuronal activation markers. This reduction in VPM thalamic activity likely reflects diminished nociceptive input and aligns with enhanced descending pain modulation via the vlOFC-vlPAG pathway.

Decreased P2 × 3 and Iba-1 expression in the vlOFC following astrocytic inhibition

P2 × 3 receptors, key purinergic receptors involved in nociceptive signaling, get elevated in astrocytes during TNP, reflecting enhanced nociceptive drive. In our study, optogenetic inhibition of astrocytic activity in the vlOFC using GFAP-NpHR significantly decreased P2 × 3 expression in the vlOFC of TNP-NpHR animals compared to TNP-ChR2 and TNP-Null groups (Fig. 6A-G). This reduction in P2 × 3 immunoreactivity suggests that suppression of astrocytic activity mitigates nociceptive inputs, creating conditions conducive to activating descending pain inhibition pathways.

We also examined Iba-1 expression, a marker of microglial activation, which is frequently upregulated in chronic pain states, contributing to neuroinflammation and sensitization of pain circuits. Our findings revealed that inhibition of vlOFC astrocytic activity significantly

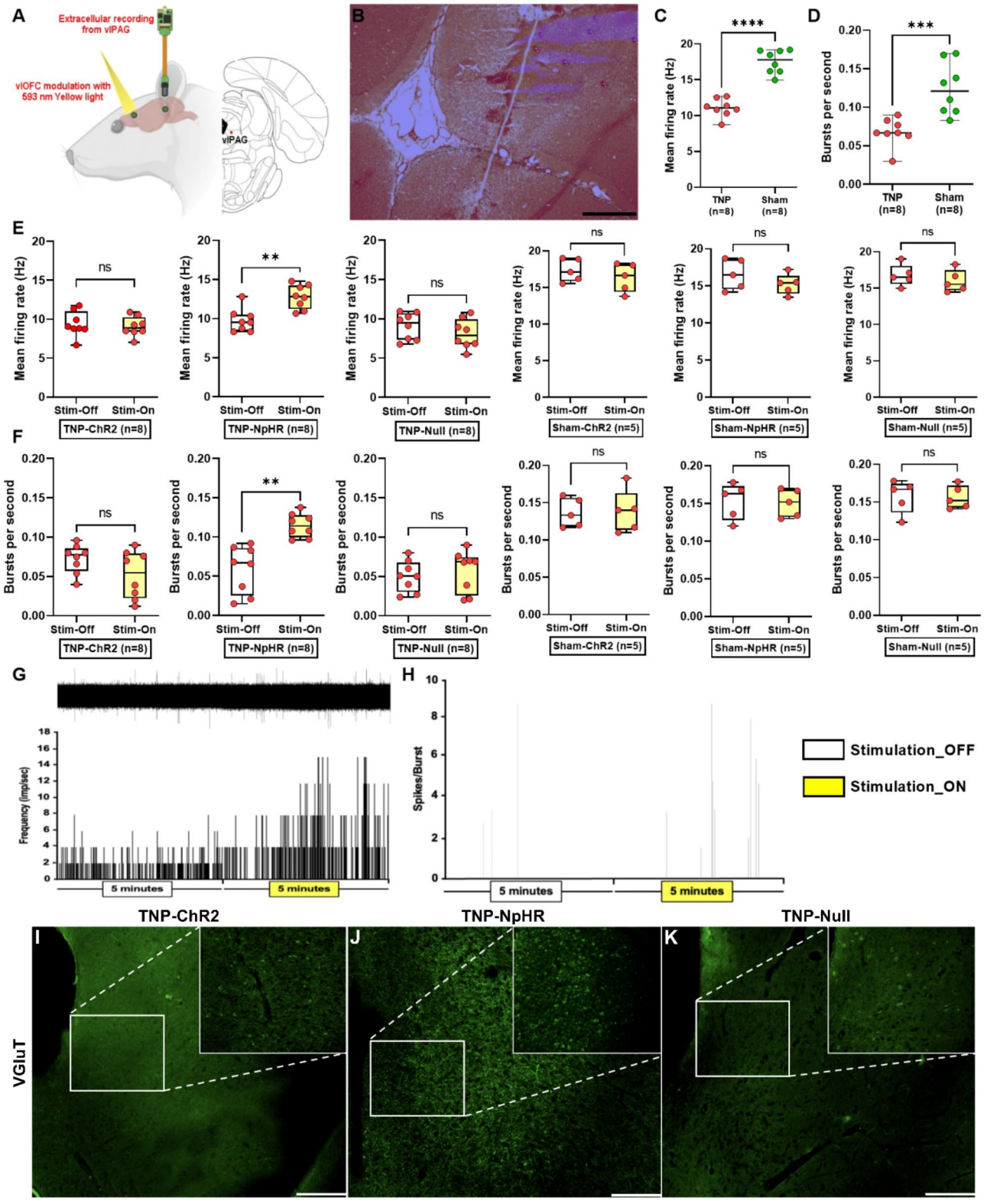

Fig. 4 (See legend on next page.)

(See figure on previous page.)

Fig. 4 Inhibition of vlOFC astrocytes increased vlPAG neural activity. **(A)** Schematic diagram of in vivo single unit extracellular recording from vlPAG. **(B)** Representative IHC image of the vlPAG coronal section shows the electrode placement in the vlPAG. **(C)** Mean firing rate from the vlPAG of TNP ($n = 8$) and sham ($n = 8$) group; unpaired *t*-test, (t, df) = (8.86, 14), $p < 0.0001$. **(D)** Burst rate from the vlPAG of TNP ($n = 8$) and sham ($n = 8$) group; unpaired *t*-test, (t, df) = (4.19, 14), $p < 0.001$. **(E)** Increased mean firing rate of vlPAG in response to optogenetic inhibition of vlOFC astrocytes in the TNP-NpHR group (paired *t*-test). **(F)** Increased burst rate of vlPAG in response to optogenetic inhibition of vlOFC astrocytes in the TNP-NpHR group (paired *t*-test). **(G)** Representative vlPAG discharge (lower, presented in frequency, impulse per second) with raw traces (upper) during stimulation-off and stimulation-on conditions in the TNP-NpHR group. **(H)** Representative burst traces of the TNP-NpHR group from the vlPAG during stimulation-off and stimulation-on conditions in vlOFC astrocytes. **(I-K)** Representative immunofluorescence image of VGluT-positive neurons in the vlPAG of TNP-ChR2 **(I)**, TNP-NpHR **(J)**, and TNP-Null **(K)** group in response to optogenetic inhibition of vlOFC astrocytes

reduced Iba-1 expression in TNP-NpHR animals compared to TNP-ChR2 and TNP-Null groups (Fig. 6H-Q). By decreasing microglial-astrocytic communication, neuroinflammatory signals that perpetuate pain were likely diminished in the TNP-NpHR group. This reduction in inflammation further enhances the environment for activating descending pain modulation pathways.

Discussion

In this study, we investigated the role of astrocytes in the vlOFC in modulating descending pain pathways and their therapeutic potential in alleviating TNP. Using an optogenetic approach, we selectively inhibited hyperactive astrocytes in the vlOFC, which led to significant restoration of descending pain modulation. This was evidenced by enhanced glutamatergic activity in the vlPAG, as shown by increased neuronal firing rates and burst activity, and by the attenuation of hyperactive spinothalamic relay activity in the VPM thalamus, reflected in reduced firing rates, burst activity, and c-Fos expression. Behaviorally, these mechanistic changes corresponded to the alleviation of nociceptive hypersensitivity in the EVF and CH tests, along with reduced anxiety-like behaviors in the EPM test. The suppression of astrocytic hyperactivity in the vlOFC restored its glutamatergic output, enhancing vlPAG activity and improving descending pain modulation. Therefore, these findings highlight that inhibiting vlOFC astrocytic activity rebalances excitatory-inhibitory dynamics across cortical and subcortical pain-modulatory networks, mitigating hyperalgesia and anxiety associated with TNP and advancing our understanding of astrocytes as potential therapeutic targets in TNP management.

Trigeminal nerve injury, a hallmark of TNP, is characterized by orofacial hyperalgesia, heightened nociceptive responses, and increased neuropeptide expression, accompanied by astrocytic hyperactivation [10, 29]. Astrocytic hyperactivity has been shown to contribute to behavioral hyperalgesia commonly observed in TNP, as well as anxiety-like responses that are often secondary to pain [24, 39]. These pathological features are particularly evident in rodent models of CCI-ION, which effectively replicate key aspects of TNP [20, 21]. The ION is a purely sensory nerve in rodents, originating from the second branch of the trigeminal nerve, which is critical for facial tactile and pain sensation. In clinical cases, drug-resistant trigeminal pain often involves the second and third branches of the trigeminal nerve and disrupts sensory transmission [1, 19]. Consistent with these observations, our study demonstrated that CCI-ION animals exhibited reduced nociceptive thresholds, enhanced anxiety-like behaviors, and elevated GFAP expression in vlOFC, a marker of astrocytic activation [53]. This astrocytic activation amplifies nociceptive signaling by regulating neurotransmitter dynamics, such as glutamate and GABA, while perpetuating neuroinflammatory responses, including P2 × 3 and Iba-1 activation, which disrupt the excitatory-inhibitory balance in critical pain-modulatory regions and sustain CNP [5, 15, 32, 33].

The vlOFC plays a pivotal role in descending pain modulation through its glutamatergic projections to the vlPAG. In CNP, the function of the vlOFC becomes significantly impaired, as evidenced by reduced glutamatergic output to the vlPAG [17, 44, 52]. This disruption is largely attributed to astrocytic hyperactivity, which induces profound changes in neurotransmitter dynamics and neuronal activity within the vlOFC. Hyperactive astrocytes excessively uptake extracellular glutamate via high-affinity transporters, such as GLT-1 and GLAST, resulting in a depletion of synaptic glutamate. This reduction in glutamate availability dampens the activation of postsynaptic NMDA and AMPA receptors on excitatory neurons, thereby suppressing glutamatergic output [12, 17, 40]. Concurrently, astrocytes can synthesize and release GABA through the enzymatic conversion of glutamate or by metabolizing putrescine, leading to increased extracellular GABA levels. This enhances inhibitory signaling by activating GABA_A and GABA_B receptors on neighboring neurons, further shifting the excitatory-inhibitory balance toward inhibition [16, 36]. In addition to modulating neurotransmitter availability, astrocytes release gliotransmitters such as ATP, which is converted extracellularly to adenosine. Adenosine acts on presynaptic A1 receptors to inhibit glutamate release from excitatory neurons while promoting GABA release from inhibitory neurons, thereby reinforcing inhibitory signaling [34, 43]. Intracellular calcium waves within astrocytes further amplify these effects by selectively interacting with GABAergic neurons, enhancing their activity through paracrine signaling and gap junctions.

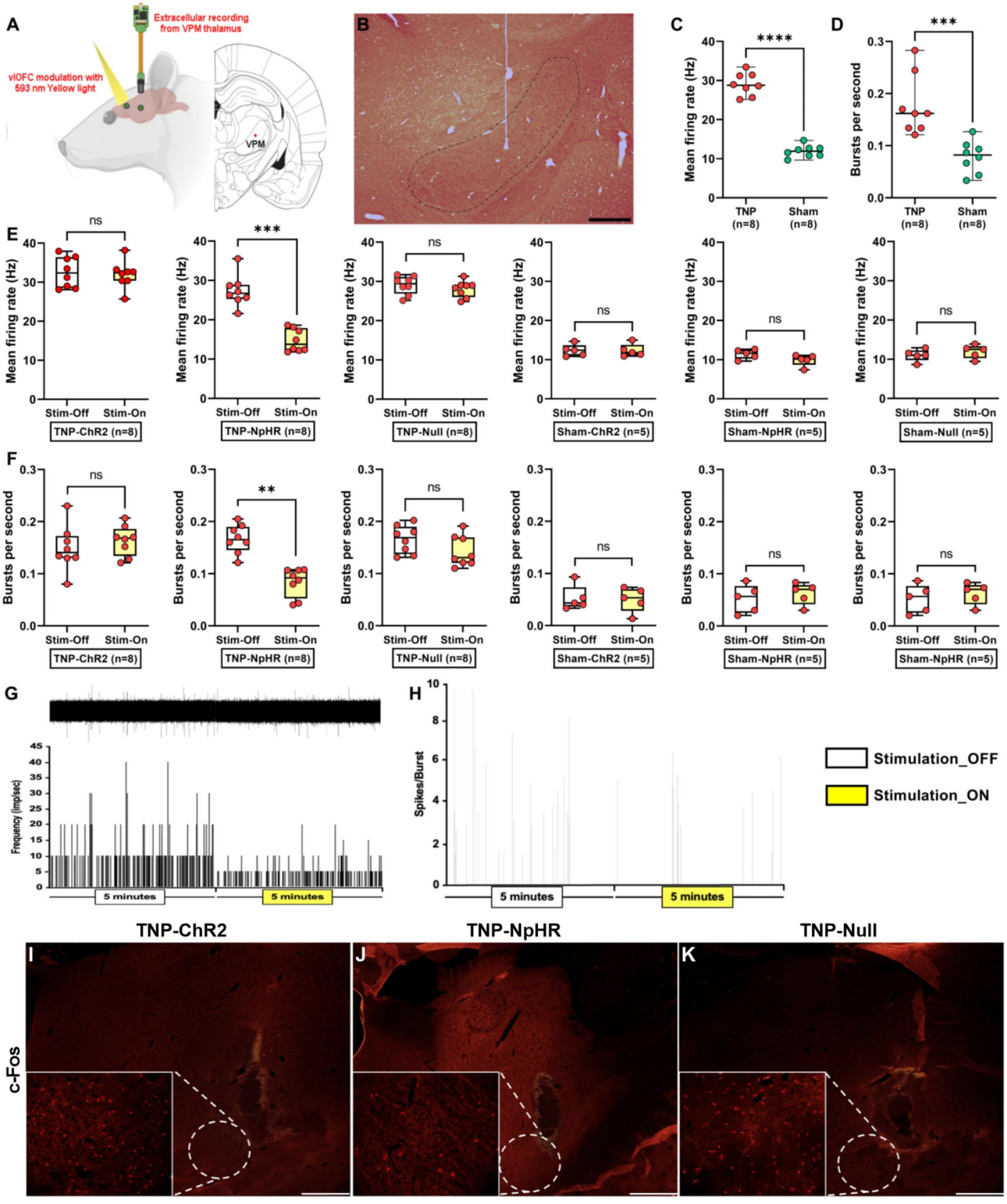

Fig. 5 (See legend on next page.)

(See figure on previous page.)

Fig. 5 Inhibition of vlOFC astrocytes reduced VPM thalamic hyperactivity. **(A)** Schematic diagram of in vivo single unit extracellular recording from VPM thalamus. **(B)** Representative IHC image of the VPM thalamus coronal section shows the electrode placement in the vlPAG. **(C)** Mean firing rate from the VPM thalamus of TNP ($n=8$) and sham ($n=8$) group; unpaired *t*-test, (t, df) = (14.92, 14), $p<0.0001$. **(D)** Burst rate from the VPM thalamus of TNP ($n=8$) and sham ($n=8$) group; unpaired *t*-test, (t, df) = (4.24, 14), $p<0.001$. **(E)** Decreased mean firing rate of VPM thalamus in response to optogenetic inhibition of vlOFC astrocytes in the TNP-NpHR group (paired *t*-test). **(F)** Decreased burst rate of VPM thalamus in response to optogenetic inhibition of vlOFC astrocytes in the TNP-NpHR group (paired *t*-test). **(G)** Representative VPM thalamic discharge (lower, presented in frequency, impulse per second) with raw traces (upper) during stimulation-off and stimulation-on conditions in the TNP-NpHR group. **(H)** Representative burst traces of the TNP-NpHR group from the VPM thalamus during stimulation-off and stimulation-on conditions in vlOFC astrocytes. **(I-K)** Representative immunofluorescence image of c-Fos-positive expression from the VPM thalamus of TNP-ChR2 (I), TNP-NpHR (J), and TNP-Null (K) group in response to optogenetic inhibition of vlOFC astrocytes

This increased GABAergic tone suppresses local excitatory circuits, compounding the reduction in glutamatergic output from the vlOFC to the vlPAG [23]. Astrocytic hyperactivity also alters the extracellular ionic environment, actively buffering potassium (K+) and releasing hydrogen ions (H+), which hyperpolarize glutamatergic neurons, reducing their excitability. Simultaneously, changes in chloride gradients enhance the activity of GABAergic neurons, further tipping the balance in favor of inhibition [49]. Consequently, the vlOFC's regulatory role over the vlPAG is impaired, perpetuating the chronic pain condition observed in CCI-ION animals. These findings emphasize the mechanistic role of astrocytes in modulating neurotransmitter dynamics within the vlOFC-vlPAG pathway and their contribution to the persistence of pain states in CNP.

To investigate vlOFC astrocytic activity in TNP and its antinociceptive potential, we used optogenetic inhibition in this study. The descending pain processing pathway, which modulates and suppresses pain signals at multiple CNS levels, represents a key therapeutic target for neuropathic pain. Unlike ascending pathways, which primarily transmit nociceptive signals, descending pathways actively regulate pain perception, making them critical for interventions [35]. The vlOFC, as a key node in this pathway, provides insights into pain modulation and resilience. Recent advancements in non-invasive neuromodulation, such as transcranial light delivery, offer precise, non-invasive methods to modulate cortical brain activity safely and effectively. Innovations like near-infrared opsins and sono-optogenetics further enhance optogenetic interventions by improving light penetration and the modulation of specific neurons and glial cells [4, 6, 30, 42, 45, 50, 54]. Anatomically, the vlOFC, located in the ventrolateral prefrontal cortex, is more accessible compared to deeper subcortical structures like the thalamus, vlPAG, or TNC, reducing risks associated with invasive targeting. Its accessibility, coupled with its established role in descending pain pathways, highlights the vlOFC as a promising and clinically viable target for non-invasive, patient-friendly neuromodulatory interventions in neuropathic pain management.

Our study demonstrated that optogenetic inhibition of astrocytes in the vlOFC effectively alleviated behavioral hypersensitivity in the CCI-ION rat model by modulating critical mechanisms involved in pain processing. This inhibition led to a marked enhancement of glutamatergic expression within the vlOFC and a concurrent reduction in the expression of P2 × 3 and Iba-1, both of which are crucial markers of nociceptive signaling and neuroinflammation. P2 × 3, a purinergic receptor expressed in neurons and glial cells, plays a significant role in mediating ATP-driven nociceptive signaling. The propagation of calcium ion waves inside astrocytes is thought to be intrinsic to ATP release, forming a foundation for intercellular communication. Recent work suggests that similar communication may also take place between astrocytes and neurons, highlighting a bidirectional mechanism where astrocytic ATP release influences neuronal activity and vice versa. The observed decrease in P2 × 3 expression following astrocytic inhibition suggests reduced extracellular ATP availability, leading to the attenuation of nociceptive inputs. This reduction in ATP signaling likely disrupts the pathological amplification of pain signals mediated by the astrocyte-neuron interaction, contributing to the observed behavioral improvements. These findings further emphasize the role of astrocytic calcium signaling and ATP release as pivotal components in nociceptive modulation [13, 27]. Similarly, Iba-1, a marker of microglial activation, was significantly reduced, indicating a suppression of microglial-driven neuroinflammatory processes. Since activated microglia release pro-inflammatory cytokines that sensitize pain pathways, this reduction in Iba-1 underscores the role of astrocytic inhibition in dampening the inflammatory cascade associated with chronic neuropathic pain [31]. These changes likely resulted from the restoration of the excitatory-inhibitory balance within the vlOFC, driven by reduced glutamate uptake by astrocytes.

Restoring the excitatory-inhibitory balance in the vlOFC facilitated enhanced glutamatergic signaling, which played a pivotal role in strengthening the vlOFC's glutamatergic projections to the vlPAG [8, 17, 52]. Electrophysiological analysis confirmed this reactivation, showing increased neuronal firing rates and burst activity in the vlPAG. These changes indicate heightened excitatory drive from the vlOFC, likely due to improved synaptic glutamate signaling. The elevated burst activity is

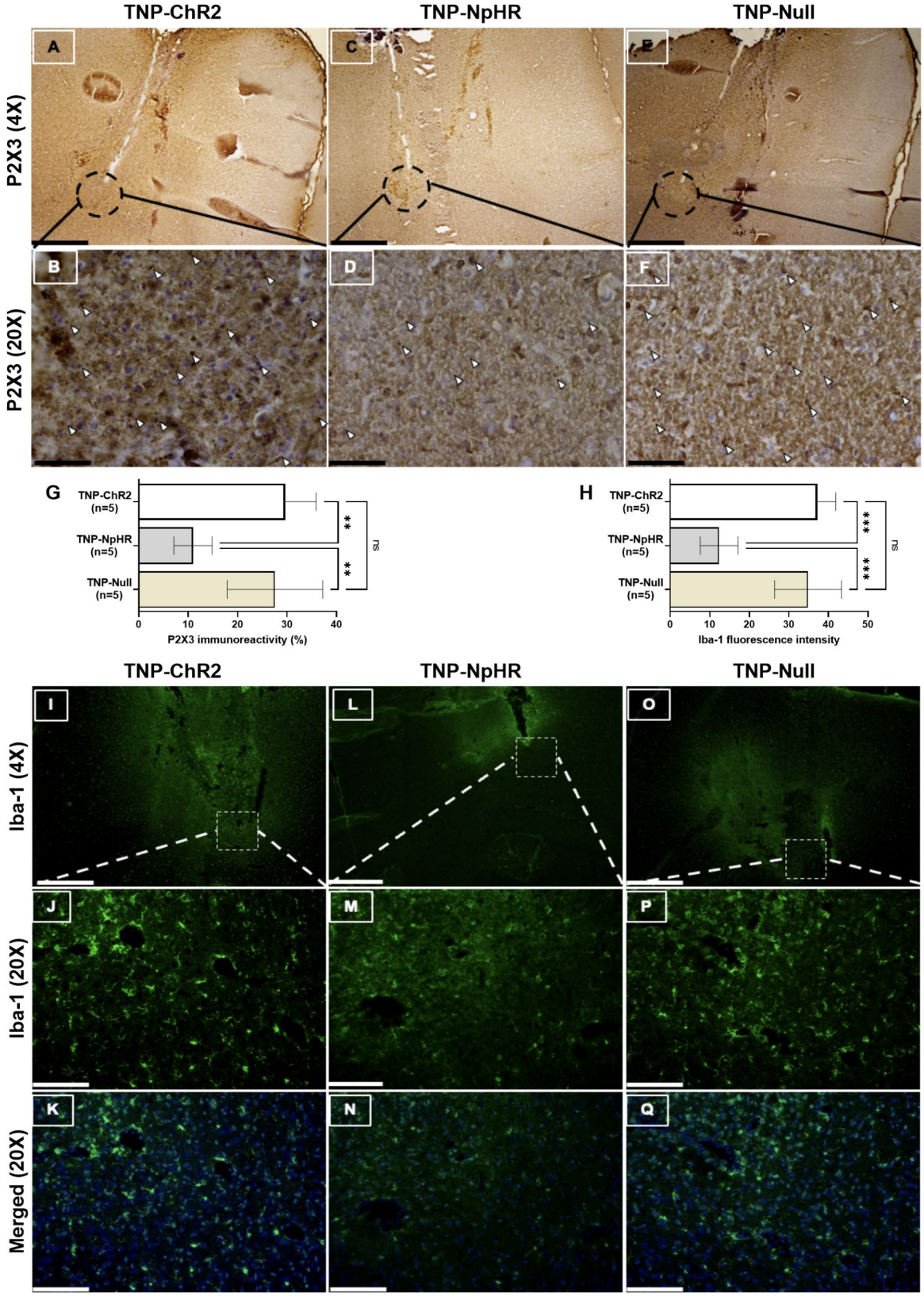

Fig. 6 (See legend on next page.)

(See figure on previous page.)

Fig. 6 P2 × 3 immunoreactivity and Iba-1 fluorescence intensity in response to astrocyte-specific vlOFC optogenetic inhibition. **(A-F)** Representative immunohistochemistry images showing P2 × 3 expression in the vlOFC of TNP-ChR2 (**A, B**), TNP-NpHR (**C, D**) and TNP-Null (**E, F**) groups in response to optic stimulation. Scale bar = 200 µm (**A, C, E**); 50 µm (**B, D, F**). **(G)** Quantification of P2 × 3 immunoreactivity in the vlOFC of TNP-ChR2 ($n = 5$), TNP-NpHR ($n = 5$), and TNP-Null ($n = 5$) groups; ordinary one-way ANOVA, F (2, 12) = 10.70, ** $p < 0.01$. **(H)** Quantification of Iba-1 immunofluorescence intensity in the vlOFC of TNP-ChR2 ($n = 5$), TNP-NpHR ($n = 5$), and TNP-Null ($n = 5$) groups; ordinary one-way ANOVA, F (2, 12) = 24.36, *** $p < 0.001$. Data were presented as the e mean ± SD. (**I-K**) Representative immunofluorescence image of Iba-1-positive expression of TNP-ChR2 group. (**L-N**) Representative immunofluorescence image of Iba-1-positive expression of TNP-NpHR group. (**O-Q**) Representative immunofluorescence image of Iba-1-positive expression of TNP-Null group. Scale bar = 200 µm (**I, L, O**); 50 µm (**J-K, M-N, P-Q**)

particularly significant, as burst firing is associated with enhanced neural communication and increased synaptic efficacy, suggesting a more robust transmission of inhibitory pain signals from the vlPAG to subsequent pain processing centers. Immunohistochemical analysis further supported these findings, showing increased glutamatergic expression in the both vlOFC and vlPAG, which aligns with the functional improvement in these regions [11, 46, 48]. The impact of the reactivated vlOFC-vlPAG pathway extended downstream to the VPM thalamus, a key relay in the spinothalamic tract responsible for transmitting orofacial nociceptive signals to higher brain centers. The strengthened descending modulation suppressed the hyperactive thalamic outputs that are characteristic of neuropathic pain states. This suppression was evidenced by reduced neuronal firing rates and burst activity in the VPM, indicating diminished nociceptive transmission. Moreover, decreased c-Fos expression, a marker of neuronal activation, further corroborated the reduction in thalamic hyperactivity. These findings suggest that the reactivation of the vlOFC-vlPAG pathway exerted inhibitory control over the VPM, dampening its excitatory outputs and effectively mitigating the amplification of pain signals within the ascending pain pathway [22, 24]. These findings highlight the pivotal role of astrocytic inhibition in restoring descending pain modulation pathways, effectively linking vlOFC astrocytic activity to broader neural networks involved in both descending and ascending pain regulation.

In contrast, optogenetic excitation of vlOFC astrocytes and null virus controls did not significantly affect TNP-related responses. Astrocytic excitation likely exacerbated hyperactivity, leading to excessive glutamate clearance, reduced synaptic glutamate availability, and impaired glutamatergic activation in the vlOFC. This disruption weakened excitatory input to the vlPAG, compromising the descending pain inhibitory pathway. The null virus group, lacking functional astrocytic modulation, served as a control and confirmed the specificity of astrocytic inhibition in driving the observed therapeutic effects. Taken together, these findings emphasize the critical role of astrocytic regulation in the vlOFC for restoring descending pain modulation, alleviating hyperalgesia, and mitigating neuroinflammation.

In our study, there are a few limitations. We only examined female animals. The animals did not receive any analgesics post-surgery to avoid anticipatory analgesic effects on the neuropathic pain process. Anesthetic drugs might have an impact on neural discharge during neural activity recording; however, we provoked the ipsilateral whisker pads with von Frey filaments to avoid such influences.

Conclusion

This study highlights the critical role of astrocytes in the vlOFC in modulating descending pain pathways and their therapeutic potential for alleviating TNP. While astrocytes are essential for maintaining glutamate homeostasis under normal conditions, our findings demonstrate that selective inhibition of astrocytic hyperactivity in the CCI-ION model may contribute to modulating the excitatory-inhibitory balance, potentially influencing glutamatergic signaling and reactivating the vlOFC-vlPAG pathway. This reactivation led to improved descending pain modulation, attenuation of hyperactive spinothalamic relay activity in the VPM thalamus, and alleviation of nociceptive hypersensitivity and behavioral symptoms. By targeting astrocytes, we provide evidence for a dual mechanism of pain modulation: (1) suppression of glial-driven neuroinflammation and excessive inhibitory signaling, and (2) restoration of neuronal excitatory signaling critical for functional connectivity within descending pain pathways. This integrated approach highlights the interplay between astrocytic regulation and neuronal activity in resolving TNP, addressing a key limitation of neuron-focused interventions that overlook glial contributions. The vlOFC's anatomical accessibility enhances the translational potential of this strategy, making it feasible for non-invasive neuromodulatory techniques. Future research should explore the long-term efficacy of astrocytic inhibition in the vlOFC, particularly its impact on the cognitive and emotional dimensions of TNP, to develop comprehensive and patient-centric therapies targeting both sensory and neuroinflammatory components of this debilitating condition.

Abbreviations

TNP	Trigeminal Neuropathic Pain
vlOFC	Ventrolateral Orbitofrontal Cortex
vlPAG	Ventrolateral Periaqueductal Gray
VPM	Ventroposterior Medial Thalamus
CCI	ION-Chronic Constriction Injury of the Infraorbital Nerve
GFAP	Glial Fibrillary Acidic Protein
eNpHR	Enhanced Halorhodopsin

ChR2	Channelrhodopsin-2
AAV	Adeno-Associated Virus
mCherry	A fluorescent protein used as a reporter
CNS	Central Nervous System
TG	Trigeminal Ganglion
CGRP	Calcitonin Gene-Related Peptide
P2X3	Purinergic Receptor 3
Iba	1-Ionized Calcium Binding Adapter Molecule 1
OAT	Open Arm Time
OAE	Open Arm Entries
EPM	Elevated Plus Maze
EVF	Electronic von Frey
IFC	Immunofluorescence
DAPI	4′,6-diamidino-2-phenylindole (a DNA stain)
SD	Standard Deviation
ANOVA	Analysis of Variance
ATP	Adenosine Triphosphate
pERK	Phosphorylated Extracellular Signal-Regulated Kinase
CREB	cAMP Response Element-Binding Protein
H&E	Hematoxylin and Eosin (a staining technique)
DAB	Diaminobenzidine
ABC	Avidin-Biotin Complex
VGLUT2	Vesicular Glutamate Transporter 2

Supplementary Information

The online version contains supplementary material available at https://doi.org/10.1186/s10194-025-01977-6.

Supplementary Material 1: Fig. 1. Experimental timeline and study design. Fig. 2. CGRP expression in the trigeminal ganglion post-CCI-ION surgery. Fig. 3. IFC analysis showing viral vector transfection efficiency in the vlOFC. Fig. 4. Immunofluorescence analysis of vlOFC glutamatergic neurons. Table 1. Behavior test results of the TNP, sham, and naive-control groups after CCI-ION surgery. Table 2. Behavioral responses of the TNP-ChR2, TNP-NpHR, TNP-null, Sham-ChR2, Sham-NpHR, and Sham-null groups with and without optogenetic stimulation. Table 3. In vivo single unit extracellular recording from the vlPAG of TNP-ChR2, TNP-NpHR, TNP-null, Sham-ChR2, Sham-NpHR, and Sham-null groups with optic stimulation OFF and ON condition. Table 4. In vivo single unit extracellular recording from the VPM thalamus of TNP-ChR2, TNP-NpHR, TNP-null, Sham-ChR2, Sham-NpHR, and Sham-Null groups with optic stimulation OFF and ON condition. Table 5. Key resources table.

Acknowledgements
Not applicable.

Author contributions
J.I. and M.T.R. conceptualized the study. J.I. selected the experimental protocols. M.T.R. and M.A. performed the behavior tests. M.T.R. and M.A. performed animal surgery. M.T.R. and M.A. conducted electrophysiology. J.I. and Y.S.P. analyzed and interpreted the electrophysiology and immunofluorescence data. J.I. and M.T.R. wrote the manuscript. J.I. prepared the revision files. H.K.K., E.K., and Y.S.P. read and approved the final version of the manuscript.

Funding
This work was supported by the National Research Foundation of Korea (NRF2023R1A2C1008079), and the Brain Korea 21 FOUR of the National Research Foundation of Korea funded by the Ministry of Education (No. 5199990614277).

Data availability
No datasets were generated or analysed during the current study.

Declarations

Ethical approval
All experiments and animal management were performed in accordance with the ethical guidelines of the International Association for the Study of Pain, approved by Chungbuk National University's Animal Care and Use Committee (IACUC) (CBNUA-25-0011-02) and the reporting in the manuscript follows the recommendations in the ARRIVE guidelines. Experiments were carried out at the Laboratory Animal Research Center of Chungbuk National University during the light hours and every effort was made to minimize the suffering and number of animals in this study.

Consent for publication
Not applicable.

Competing interests
The authors declare no competing interests.

Author details
[1]Program in Neuroscience, College of Medicine, Chungbuk National University, Cheongju 28644, Republic of Korea
[2]Department of Medicine and Microbiology, College of Medicine, Chungbuk National University, Cheongju 28644, Republic of Korea
[3]Department of Neuroscience and Regenerative Medicine, Medical College of Georgia, Augusta University, Augusta, GA, USA
[4]Department of Neurosurgery, Chungbuk National University Hospital, Cheongju 28644, Republic of Korea

Received: 13 January 2025 / Accepted: 10 February 2025
Published online: 25 February 2025

References

1. Araya EI, Carvalho EC, Andreatini R, Zamponi GW, Chichorro JG (2022) Trigeminal neuropathic pain causes changes in affective processing of pain in rats. Mol Pain 18:17448069211057750
2. Bang J, Kim HY, Lee H (2016) Optogenetic and chemogenetic approaches for studying astrocytes and gliotransmitters. Experimental Neurobiol 25(5):205
3. Bangash TH (2011) Trigeminal neuralgia: frequency of occurrence in different nerve branches. Anesthesiology pain Med 1(2):70
4. Bedbrook CN, Yang KK, Robinson JE, Mackey ED, Gradinaru V, Arnold FH (2019) Machine learning-guided channelrhodopsin engineering enables minimally invasive optogenetics. Nat Methods 16(11):1176–1184
5. Boué-Grabot E, Pankratov Y (2017) Modulation of central synapses by astrocyte-released ATP and postsynaptic P2X receptors. Neural Plast 2017(1):9454275
6. Chen S, Weitemier AZ, Zeng X, He L, Wang X, Tao Y, Huang AJ, Hashimotodani Y, Kano M, Iwasaki H (2018) Near-infrared deep brain stimulation via upconversion nanoparticle–mediated optogenetics. Science 359(6376):679–684
7. Cheng T, Xu Z, Ma X (2022) The role of astrocytes in neuropathic pain. Front Mol Neurosci 15:1007889
8. Dang Y, Zhao Y, Xing B, Zhao X, Huo F, Tang J, Qu C, Chen T (2010) The role of dopamine receptors in ventrolateral orbital cortex-evoked anti-nociception in a rat model of neuropathic pain. Neuroscience 169(4):1872–1880
9. Davies AJ, Kim YH, Oh SB (2010) Painful neuron-microglia interactions in the trigeminal sensory system. Open Pain J 3 (1)
10. Dieb W, Hafidi A (2013) Astrocytes are involved in trigeminal dynamic mechanical allodynia: potential role of D-serine. J Dent Res 92(9):808–813
11. Elina K, Oh BH, Islam J, Kim S, Park YS (2021) Activation of CamKIIα expressing neurons on ventrolateral periaqueductal gray improves behavioral hypersensitivity and thalamic discharge in a trigeminal neuralgia rat model. J Headache Pain 22(1):47
12. Escartin C, Brouillet E, Gubellini P, Trioulier Y, Jacquard C, Smadja C, Knott GW, Kerkerian-Le Goff L, Déglon N, Hantraye P (2006) Ciliary neurotrophic factor activates astrocytes, redistributes their glutamate transporters GLAST and GLT-1 to raft microdomains, and improves glutamate handling in vivo. J Neurosci 26(22):5978–5989
13. Fields RD, Burnstock G (2006) Purinergic signalling in neuron–glia interactions. Nat Rev Neurosci 7(6):423–436
14. Guo G, Liu Y, Ren S, Kang Y, Duscher D, Machens H-G, Chen Z (2018) Comprehensive analysis of differentially expressed microRNAs and mRNAs in dorsal root ganglia from streptozotocin-induced diabetic rats. PLoS ONE 13(8):e0202696
15. Héja L, Barabás P, Nyitrai G, Kékesi KA, Lasztóczi B, Tőke O, Tárkányi G, Madsen K, Schousboe A, Dobolyi Á (2009) Glutamate uptake triggers transporter-mediated GABA release from astrocytes. PLoS ONE 4(9):e7153

16. Héja L, Nyitrai G, Kékesi O, Dobolyi Á, Szabó P, Fiáth R, Ulbert I, Pál-Szenthe B, Palkovits M, Kardos J (2012) Astrocytes convert network excitation to tonic inhibition of neurons. BMC Biol 10:1–21
17. Huang J, Zhang Z, Gambeta E, Chen L, Zamponi GW (2021) An orbitofrontal cortex to midbrain projection modulates hypersensitivity after peripheral nerve injury. Cell Rep 35 (4)
18. Islam J, Elina K, Park YS (2022) Recent update on trigeminal neuralgia. J Korean Soc Stereotact Funct Neurosurg 18(1):9–19
19. Islam J, Kc E, Kim S, Chung MY, Park KS, Kim HK, Park YS (2023a) Optogenetic Inhibition of Glutamatergic Neurons in the dysgranular posterior insular cortex modulates Trigeminal Neuropathic Pain in CCI-ION rat. Neuromol Med 25(4):516–532
20. Islam J, Kc E, Kim S, Kim HK, Park YS (2021) Stimulating gabaergic neurons in the nucleus accumbens core alters the trigeminal neuropathic pain responses in a rat model of infraorbital nerve injury. Int J Mol Sci 22(16):8421
21. Islam J, Kc E, Oh BH, Kim S, Hyun S-h, Park YS (2020) Optogenetic stimulation of the motor cortex alleviates neuropathic pain in rats of infraorbital nerve injury with/without CGRP knock-down. J Headache Pain 21:1–13
22. Islam J, Kc E, So KH, Kim S, Kim HK, Park YY, Park YS (2023b) Modulation of trigeminal neuropathic pain by optogenetic inhibition of posterior hypothalamus in CCI-ION rat. Sci Rep 13(1):489
23. Jacob PF, Vaz SH, Ribeiro JA, Sebastiao AM (2014) P2Y1 receptor inhibits GABA transport through a calcium signalling-dependent mechanism in rat cortical astrocytes. Glia 62(8):1211–1226
24. Kc E, Islam J, Kim HK, Park YS (2023) GFAP-NpHR mediated optogenetic inhibition of trigeminal nucleus caudalis attenuates hypersensitive behaviors and thalamic discharge attributed to infraorbital nerve constriction injury. J Headache Pain 24(1):137
25. Kc E, Islam J, Lee G, Park YS (2024) Optogenetic Approach in Trigeminal Neuralgia and potential concerns: preclinical insights. Mol Neurobiol 61(3):1769–1780
26. Kim Y, Park J, Choi YK (2019) The role of astrocytes in the central nervous system focused on BK channel and heme oxygenase metabolites: a review. Antioxidants 8(5):121
27. Koizumi M, Asano S, Furukawa A, Hayashi Y, Hitomi S, Shibuta I, Hayashi K, Kato F, Iwata K, Shinoda M (2021) P2X3 receptor upregulation in trigeminal ganglion neurons through TNFα production in macrophages contributes to trigeminal neuropathic pain in rats. J Headache Pain 22(1):31
28. Koizumi S, Fujishita K, Inoue K (2005) Regulation of cell-to-cell communication mediated by astrocytic ATP in the CNS. Purinergic Signalling 1:211–217
29. Korczeniewska OA, Kohli D, Benoliel R, Baddireddy SM, Eliav E (2022) Pathophysiology of post-traumatic trigeminal neuropathic pain. Biomolecules 12(12):1753
30. Lee SH, Kim J, Shin JH, Lee HE, Kang I-S, Gwak K, Kim D-S, Kim D, Lee KJ (2018) Optogenetic control of body movements via flexible vertical light-emitting diodes on brain surface. Nano Energy 44:447–455
31. Leinders M, Knaepen L, De Kock M, Sommer C, Hermans E, Deumens R (2013) Up-regulation of spinal microglial Iba-1 expression persists after resolution of neuropathic pain hypersensitivity. Neurosci Lett 554:146–150
32. Liu S, Cheng H, Cui L, Jin L, Li Y, Zhu C, Ji Q, Tang J (2024) Astrocytic purinergic signalling contributes to the development and maintenance of neuropathic pain via modulation of glutamate release. J Neurochem 168(11):3727–3744
33. Mah W, Lee SM, Lee J, Bae JY, Ju JS, Lee CJ, Ahn DK, Bae YC (2017) A role for the purinergic receptor P2X3 in astrocytes in the mechanism of craniofacial neuropathic pain. Sci Rep 7(1):13627
34. Matos M, Bosson A, Riebe I, Reynell C, Vallée J, Laplante I, Panatier A, Robitaille R, Lacaille J-C (2018) Astrocytes detect and upregulate transmission at inhibitory synapses of somatostatin interneurons onto pyramidal cells. Nat Commun 9(1):4254
35. Millan MJ (2002) Descending control of pain. Prog Neurobiol 66(6):355–474
36. Müller J, Timmermann A, Henning L, Müller H, Steinhäuser C, Bedner P (2020) Astrocytic GABA accumulation in experimental temporal lobe epilepsy. Front Neurol 11:614923
37. Murphy-Royal C, Dupuis J, Groc L, Oliet SH (2017) Astroglial glutamate transporters in the brain: regulating neurotransmitter homeostasis and synaptic transmission. J Neurosci Res 95(11):2140–2151
38. Nam Y, Kim J-H, Kim J-H, Jha MK, Jung JY, Lee M-G, Choi I-S, Jang I-S, Lim DG, Hwang S-H (2016) Reversible induction of pain hypersensitivity following optogenetic stimulation of spinal astrocytes. Cell Rep 17(11):3049–3061
39. Okada-Ogawa A, Suzuki I, Sessle BJ, Chiang C-Y, Salter MW, Dostrovsky JO, Tsuboi Y, Kondo M, Kitagawa J, Kobayashi A (2009) Astroglia in medullary dorsal horn (trigeminal spinal subnucleus caudalis) are involved in trigeminal neuropathic pain mechanisms. J Neurosci 29(36):11161–11171
40. Pajarillo E, Rizor A, Lee J, Aschner M, Lee E (2019) The role of astrocytic glutamate transporters GLT-1 and GLAST in neurological disorders: potential targets for neurotherapeutics. Neuropharmacology 161:107559
41. Ren K (2010) Emerging role of astroglia in pain hypersensitivity. Japanese Dent Sci Rev 46(1):86–92
42. Sahel J-A, Boulanger-Scemama E, Pagot C, Arleo A, Galluppi F, Martel JN, Esposti SD, Delaux A, de Saint Aubert J-B, de Montleau C (2021) Partial recovery of visual function in a blind patient after optogenetic therapy. Nat Med 27(7):1223–1229
43. Shen W, Li Z, Tang Y, Han P, Zhu F, Dong J, Ma T, Zhao K, Zhang X, Xie Y (2022) Somatostatin interneurons inhibit excitatory transmission mediated by astrocytic GABAB and presynaptic GABAB and adenosine A1 receptors in the hippocampus. J Neurochem 163(4):310–326
44. Sheng H-Y, Lv S-S, Cai Y-Q, Shi W, Lin W, Liu T-T, Lv N, Cao H, Zhang L, Zhang Y-Q (2020) Activation of ventrolateral orbital cortex improves mouse neuropathic pain–induced anxiodepression. JCI Insight 5 (19)
45. Sun C, Fan Q, Xie R, Luo C, Hu B, Wang Q (2024) Tetherless Optical Neuromodulation: Wavelength from Orange-red to mid-infrared. Neurosci Bull: 1–16
46. Taati M, Tamaddonfard E (2018) Ventrolateral orbital cortex oxytocin attenuates neuropathic pain through periaqueductal gray opioid receptor. Pharmacol Rep 70(3):577–583
47. Tang J-S, Qu C-L, Huo F-Q (2009) The thalamic nucleus submedius and ventrolateral orbital cortex are involved in nociceptive modulation: a novel pain modulation pathway. Prog Neurobiol 89(4):383–389
48. Tovote P, Esposito MS, Botta P, Chaudun F, Fadok JP, Markovic M, Wolff SB, Ramakrishnan C, Fenno L, Deisseroth K (2016) Midbrain circuits for defensive behaviour. Nature 534(7606):206–212
49. Wang F, Smith NA, Xu Q, Fujita T, Baba A, Matsuda T, Takano T, Bekar L, Nedergaard M (2012) Astrocytes modulate neural network activity by Ca2+-dependent uptake of extracellular K+. Sci Signal 5(218):ra26–ra26
50. Wu X, Zhu X, Chong P, Liu J, Andre LN, Ong KS, Brinson K Jr, Mahdi AI, Li J, Fenno LE (2019) Sono-optogenetics facilitated by a circulation-delivered rechargeable light source for minimally invasive optogenetics. Proceedings of the National Academy of Sciences 116 (52):26332–26342
51. Yang S, Yu Z, Sun W, Jiang C, Ba X, Zhou Q, Xiong D, Xiao L, Deng Q, Hao Y (2020) The antiviral alkaloid berberine ameliorates neuropathic pain in rats with peripheral nerve injury. Acta Neurol Belgica 120(3):557–564
52. Zhang S, Tang J-S, Yuan B, Jia H (1997) Involvement of the frontal ventrolateral orbital cortex in descending inhibition of nociception mediated by the periaqueductal gray in rats. Neurosci Lett 224(2):142–146
53. Zhang S, Wu M, Peng C, Zhao G, Gu R (2017) GFAP expression in injured astrocytes in rats. Experimental Therapeutic Med 14(3):1905–1908
54. Zhang Y, Yang D, Nie J, Dai J, Wu H, Zheng JC, Zhang F, Fang Y (2023) Transcranial Nongenetic Neuromodulation via Bioinspired Vesicle-Enabled Precise NIR-II Optical Stimulation. Adv Mater 35(3):2208601

Publisher's note